Plant Physiology and Biochemistry 135 (2019) 411–422

Contents lists available at ScienceDirect

Plant Physiology and Biochemistry

journal homepage: www.elsevier.com/locate/plaphy

Research article

Active rearrangements in the cell wall follow polymer concentration during postharvest withering in the berry skin of *Vitis vinifera* cv. Corvina

Marianna Fasoli[a,1,2], Rossana Dell'Anna[b,2], Alessandra Amato[a], Raffaella Balestrini[c], Silvia Dal Santo[a], Francesca Monti[d,*], Sara Zenoni[a]

[a] Department of Biotechnology, University of Verona, 37134, Verona, Italy
[b] Centre for Materials and Microsystems, Micro Nano Facility, Fondazione Bruno Kessler, 38123, Trento, Italy
[c] CNR, Institute for Sustainable Plant Protection, 10125, Torino, Italy
[d] Department of Computer Science, University of Verona, 37134, Verona, Italy

ARTICLE INFO

Keywords:
Vitis vinifera
Postharvest withering
Polymer dynamics
Plant cell wall
FTIR micro-spectroscopy

ABSTRACT

During grape postharvest withering, a worldwide practice used to produce important high-quality wines, the solute concentration increases due to dehydration, and many organoleptic and quality traits, especially related to the berry skin, are affected in a cultivar-specific manner. Nevertheless, a complete comprehension of the underlying processes is still lacking.

In this work, we applied ATR-FTIR micro-spectroscopy combined with PCA to monitor cell wall biochemical changes at three stages during postharvest withering on the internal and external sides of the berry skin of the *Vitis vinifera* cv. Corvina, an important local variety of the Verona province in Italy. The obtained results were integrated by profiling xylogucans and pectins through immunohistochemistry and by genome-wide transcriptomic analysis performed at the same withering stages.

Our analysis indicates a gradual passive polymer concentration due to water loss in the first two months of postharvest withering, followed by active structural modifications in the last month of the process. Such rearrangements involve xyloglucans in the internal surface, cuticle components and cellulose in the external surface, and pectins in both surfaces. Moreover, by investigating the expression trend of cell wall metabolism-related genes, we identified several putative molecular markers associated to the polymer dynamics.

The present study represents an important step towards an exhaustive comprehension of the postharvest withering process, which is of great interest from both the biological and technological points of view.

1. Introduction

Wine grapes are generally harvested at the commercial ripening stage, when the quality parameters fulfil oenological requirements. In particular, the most important phenols and other compounds affecting wine flavour and aroma are accumulated in the hypodermal layer of the berry skin (Ortega-Regules et al., 2006; Bindon et al., 2012). To produce peculiar wine styles, the berries must undergo a post-ripening process, during which the solute concentration increases and many organoleptic traits are modified. To reach the desirable weight loss in view of winemaking, the berries may either be left on the plant beyond ripening or collected and stored in appropriate dehydrating rooms. This practice, known as postharvest withering, is of a particularly great importance in the province of Verona (North-east, Italy) to make worldwide marketed wines such as Amarone and Recioto. Corvina is the principal cultivar used for the production of these wines (Paronetto and Dellaglio, 2011). Typically, harvested Corvina berries undergo a ~3-months dehydration period during which profound transcriptomic and metabolic changes occur, which were investigated in the berry as a whole (Zamboni et al., 2008). As regards the effect of withering on the skin of the berries, a direct relation of berry features, such as size and skin texture, with the dehydration kinetics was evidenced in several varieties (Barbanti et al., 2008; Rolle et al., 2011; Giacosa et al., 2012; Rolle and Gerbi, 2013), but few studies concern the consequences of

* Corresponding author.
E-mail addresses: marianna.fasoli@ejgallo.com (M. Fasoli), dellanna@fbk.eu (R. Dell'Anna), alessandra.amato@univr.it (A. Amato), raffaella.balestrini@ipsp.cnr.it (R. Balestrini), silvia.dalsanto@univr.it (S. Dal Santo), francesca.monti@univr.it (F. Monti), sara.zenoni@univr.it (S. Zenoni).
[1] Present address: E. & J. Gallo Winery, Modesto CA, USA.
[2] contributed equally to the paper.

https://doi.org/10.1016/j.plaphy.2018.11.020
Received 24 September 2018; Received in revised form 17 November 2018; Accepted 17 November 2018
Available online 19 November 2018
0981-9428/

post-ripening or postharvest withering specifically on the berry skin metabolism and proprieties.

A significant modification of skin hardness and thickness was observed in Mondeuse berries (Rolle et al., 2009). Shiraz berries showed an increase of demethylation of skin pectins during a post-ripening period (Vicens et al., 2009). In Aleatico berries, a constant increase in pectin methylesterase (PME) activity and a peak of polygalacturonase (PG) activity upon withering was reported (Botondi et al., 2011). Similarly, a PME activity was detected at the end of withering in Erbaluce berries (Vincenzi et al., 2012), suggesting that an active pectin structural modification takes place during the last phase of the process.

More recently, it was demonstrated that postharvest withering affects pectin metabolism in a cultivar-specific manner related to the kinetics of water loss, showing a marginal impact in Sangiovese and Oseleta grapes but a more substantial effect in Corvina berries (Zoccatelli et al., 2013), where the process of water loss is slower. A very recent comparison among metabolic and transcriptomic changes in six red berry genotypes, subject to postharvest withering under the same environmental conditions, revealed that the transcriptional control of cell metabolism is active even after several months following the berry harvest and storage (Zenoni et al., 2016). Moreover, this study demonstrated that Corvina berries, which are characterized by large and thick skins with compact layers and a slow dehydration kinetic, are specifically responsive in terms of transcriptional modulation and metabolic changes (Zenoni et al., 2016), supporting the importance of the dehydration rate in determining the quality traits of dried grapes (Versari et al., 2001; Rizzini et al., 2009; Mencarelli et al., 2010). However, a complete comprehension of the processes underlying postharvest withering is still lacking.

A detailed understanding of cell wall biochemical changes and skin structure modifications occurring during postharvest withering could help in this direction. To this respect, Fourier transform infrared (FTIR) spectroscopy coupled to multivariate statistical analysis can be successfully applied since it allows the simultaneous determination of the overall molecular composition of plant cell walls (Cavagna et al., 2010; Largo-Gosens et al., 2014) and provides information on polysaccharides *in situ* without the need of extracting or solubilizing, therefore altering, the cell wall. Among various FTIR experimental techniques, attenuated total reflection (ATR) is intrinsically more sensitive to modifications in the external cell structures due to the reduced photon beam penetration depth (Burattini et al., 2008). FTIR spectroscopy was proved to be an important tool in studying the heterogeneity in cell wall structure and composition of different species and of a single species subject to different biotic or abiotic stress factors (Alonso-Simón et al., 2011). As regards grapevine, FTIR spectroscopy has been applied to leaves and roots under biotic or abiotic stress (Oliveira et al., 2009) and to alcohol insoluble residue extracts for the high-throughput analysis of fully expanded leaves and ripening berries polymer composition (Moore et al., 2014a, 2014b). Recently, we applied ATR-FTIR micro-spectroscopy combined with Principal Component Analysis (PCA) to study and monitor, for the first time, the polymer composition and evolution over ripening of intact berry skins from the Corvina grapevine variety (Fasoli et al., 2016).

Here we used the same method to monitor polymer modifications of the Corvina berry skin during postharvest withering. The results obtained by applying FTIR spectroscopy in the internal and external surfaces of the berry skin at three stages of the withering process were compared and integrated by profiling xylogucans and pectins accumulation through immunohistochemical analyses and by investigating the expression trend of cell wall metabolism-related genes at the same withering stages.

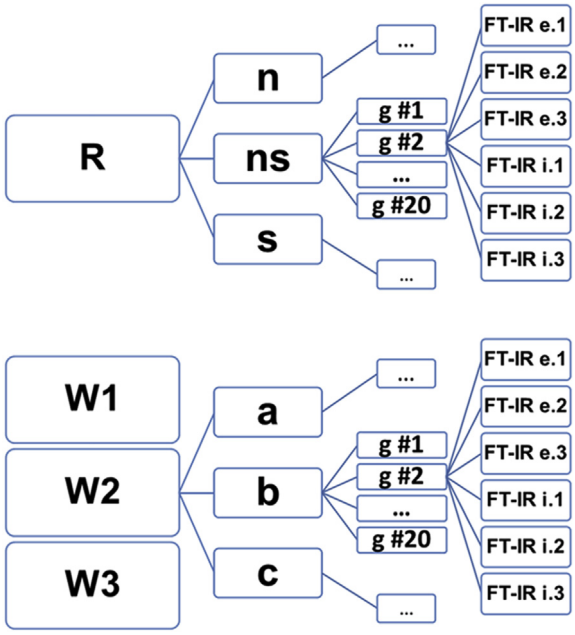

Fig. 1. Sampling strategy for FTIR analyses. The three biological replicates for the ripening stage (R) were obtained as a pool of pericarps from five clusters detached from five different vines located at the north (n), middle (ns) and south (s) sites of the vineyard. For the withering stages (W1, W2 and W3), three biological replicates were obtained as a pool of berries from five clusters taken from three different trays (a, b and c) of the same drying room. Twenty berries were collected for each replicate, i.e. 240 berries. Three point-by-point absorption spectra were acquired for the internal and for the external surfaces of the skin for each berry, i.e. 1440 single-point spectra.

2. Materials and methods

2.1. Plant material and sampling

Grape berries were collected during the 2006 growing season from a *Vitis vinifera* cv Corvina (clone 48) vineyard located in Montorio (Verona, Italy). Berries were sampled at their full ripening stage (i.e., 112 days after fruit set (R)) and during the postharvest withering process at three time points: 35 days (W1), 56 days (W2), and 91 days (W3) after harvest. Three biological replicates were taken at each time point. After collection, the berries were frozen in liquid nitrogen.

The full ripening stage was identified as the commercial ripening stage (R; 20.8° Brix) according to the E-L system modified by Coombe et al. (1995). The corresponding biological replicates were obtained from vines located at the north (n), middle (ns) and south (s) sites of the vineyard (Fig. 1). Each biological replicate was obtained as a pool of pericarps (entire berries without seeds) from five clusters detached from five different plants. After harvesting, the bunches were put on wooden trays and stored in a drying room (the so-called *fruttaio*) equipped with dehumidifying/refrigeration air-conditioning (Zanoni Impianti). The room settings mimicked the average values registered in traditional non-conditioned dehydrating rooms over the previous 10 years, i.e. gradual decrease of temperature from 16 °C to 7 °C and relative humidity not exceeding 65%. For the withering stages W1, W2 and W3, each biological replicate was obtained as a pool of berries detached from five bunches collected from different trays (a, b and c; Fig. 1) at each time point. The percentage weight loss upon withering was calculated by referring the average weight of 400 berries at each withering time point to the average weight of 400 berries at full ripening. Brix degree mean values ± SD (n = 7) expressing the total soluble solids were monitored with a PR-32 refractometer (Atago).

Optical microscopy, immuno-histochemistry and FTIR micro-spectroscopy were applied on the berry skins carefully removed from the

frozen berries.

2.2. Optical microscopy and immunofluorescence

Grapevine cv Corvina berry skins were fixed by overnight vacuum in 2% formaldehyde and 0.25% glutaraldehyde Phosphate-buffered saline (PBS; pH 7.5). Fixed materials were rinsed five times in PBS and subsequently dehydrated in four consecutive solutions containing increasing concentration of ethanol (25%, 50%, 75% and 100%). The samples were embedded by progressively substituting the xylene with Paraplast Plus (Thermo Fisher Scientific). Tissue sections (7 μm thick) were prepared with a 2035 Leica microtome (Leica Microsystems GmbH), floated on warm water, and immobilized on slides coated with Poly-L-lysine to facilitate handling. The slides were then air-dried at 37 °C. After removing the paraffin by incubating in 100% xylene (2 × 15 min) and passing quickly through decreasing concentrations of ethanol, the sections were stained with toluidine blue and viewed under a Leica DMRB optical microscope (Leica Microsystems GmbH). Cuticle has been detected using the Sudan IV staining. Skin sections were rinsed for 5 min in 70% EtOH, stained for 6 min with Sudan IV, agitating occasionally, washed in 80% EtOH for 3 min to eliminate the excess staining and then put in water.

Skin sections have been also used for immunofluorescence experiments to localize cell wall polysaccharides. Briefly, sections were blocked in a phosphate buffer containing 1% bovine serum albumin (BSA; w/v) for 30 min, incubated overnight at 4 °C with the LM19, JIM7 or CCRC-M1 and CCRC-M58 antibodies (CarboSource, http://www.ccrc.uga.edu/carbosource/CSS_mabs7-07.html), diluted 1:5 in 1% BSA, washed three times with phosphate buffer for about 30 min, saturated for 30 min with 1% (w/v) BSA in phosphate buffer, and incubated at room temperature in the dark for 3 h with a goat anti-rat IgG (for LM19 and JIM7) or a goat anti-mouse IgG (for CCRC-M1 and CCRC-M58) conjugated to fluorescein isothiocyanate (FITC) (dilution 1:60 in 1% BSA). The sections were washed as before, mounted, and observed under a Leica TCS SP2 confocal microscope, using a 40 water-immersion objective, at 496 nm (green signal) and 601 nm (red signal). No specific signal was observed in the negative control sections where primary antibody was omitted, except for the cuticle layer, which displayed unspecific auto-fluorescence (not shown).

2.3. FTIR spectra acquisition and analysis

The experimental design of FTIR measurement is shown in Fig. 1. Twenty grape berries were collected for each independent biological replicate at the full ripening stage (R) and at the three withering stages (W1, W2, W3) as described in section 2.1, i.e. 240 berries. Three point-by-point absorption spectra were acquired for the internal and for the external surfaces of the skin for each berry, i.e. 1440 single-point spectra.

Mid-infrared spectra were acquired in ATR mode in the 4000–700 cm^{-1} range at 4 cm^{-1} resolution over a 100 μm diameter area by co-adding 64 scans (acquisition time = 27 s) using a Vertex 70 Bruker spectrometer coupled to a Hyperion 3000 vis/IR microscope equipped with a photoconductive MCT detector and a 20× germanium ATR-crystal objective. Before measurement, the skin was removed from the frozen berries and thawed at room temperature. Measurements were performed on all the samples dried at the same thawing time (10 min at room temperature). To acquire the infrared signal, a small amount of water released during the thawing process was also carefully removed manually. By comparing spectra acquired on a set of fresh and thawed samples we checked that there was no significant alteration in the thawed samples with respect to the fresh ones, especially as regards absorption bands related to cell wall polymers.

Since in ATR measurements the penetration depth inside the sample is proportional to the wavelength (Griffiths and de Haseth, 1986), the usual ATR correction was applied by multiplying the absorption value at each spectral channel by the corresponding wavenumber. Due to the softness of the berry skin, the ATR objective probed cuticle and epidermal layers in measurements made on the external surface, and hypodermal cells in measurements made on the internal surface (Fasoli et al., 2016).

Data treatment was performed in the 2000-700 cm^{-1} range where we found the most interesting spectral information. Single-point absorbance spectra were baseline-corrected using the rubber band method and area-normalized. Principal Component Analysis was carried out in the R software environment (Monti et al., 2013; Team, 2015) after applying a procedure based on an automatic selection of spectra fully described elsewhere (Monti et al., 2013). Briefly, the procedure consists in iteratively discarding the single-point spectra having the lowest Pearson correlation coefficient with the average spectrum. In each cycle, the average spectrum is recalculated until all the correlation coefficients are higher than a threshold value chosen to preserve the biological variability. As a result, the spectral differences present in the original dataset are enhanced and in the PCA a higher percentage of the total variance and is described by a lower Principal Component.

The average spectra, calculated for each replicate at the full ripening stage and at the withering stages after the automatic selection of the spectra were analysed though PCA. The first two principal components in our analyses always best described the spread of the data, and the projection of the absorption spectra onto this two-dimensional principal component plane (score-score plot) allowed us to visualize the relationships among them responsible for the related captured variance. The grouping and differences in the score plot along each PC, can in turn be explained by the increasing or decreasing intensity of certain absorption bands in the corresponding loading plot.

2.4. Transcriptome analysis

The expression profiles of genes related to cell wall were analysed by retrieving from the *Vitis vinifera* cv Corvina global expression atlas (Fasoli et al., 2012) the samples related to the berry skin tissue at the same phenological stages analysed in this work.

Genes differentially expressed among these samples were evaluated by the multiclass Significance Analysis of Microarray (SAM) statistical technique, using 4 classes and a False Discovery Rate (FDR) of 1% (TMeV software suite v4.8). SAM identified 4108 statistically significant genes that were further analysed by Gene Ontology (GO) annotation. As a result, we obtained 81 differentially expressed genes displaying a Biological Process GO related to cell wall metabolism. The expression profiles of the selected 81 genes were firstly analysed by the Figure of Merit (FOM) analysis, obtaining 5 as the cluster number that maximized the predictive power of the following K-Means Cluster (KMC) analysis. KMC analysis was thus performed using 5 clusters and a metric based on the Pearson's correlation coefficient. FOM, KMC and cluster-specific heat maps were obtained using the TMeV software suite v4.8. Averaged profiles of cluster-specific genes were plotted by days after harvest using the smoothed conditional means function (level of confidence = 0.95) of the R package ggplot2 v2.2.1 (Wickham, 2009).

3. Results and discussion

3.1. Morphological alterations in the berry skin during postharvest withering

Images of the Corvina berries at the full ripening stage and at the three withering stages, as described in section 2.1 are shown in Fig. 2A. The dehydration kinetic was monitored up to the final withering stage, resulting in a ~21% weight-loss. The Brix degree value expressing the total soluble solid at each withering stage showed a pronounced increase from R to W1, whereas it mildly increases from W1 to W3 (Fig. 2A).

In the skin sections stained with toluidine blue, the cuticle, the epidermis and the hypodermal layers can be visualized (Fig. 2B). The

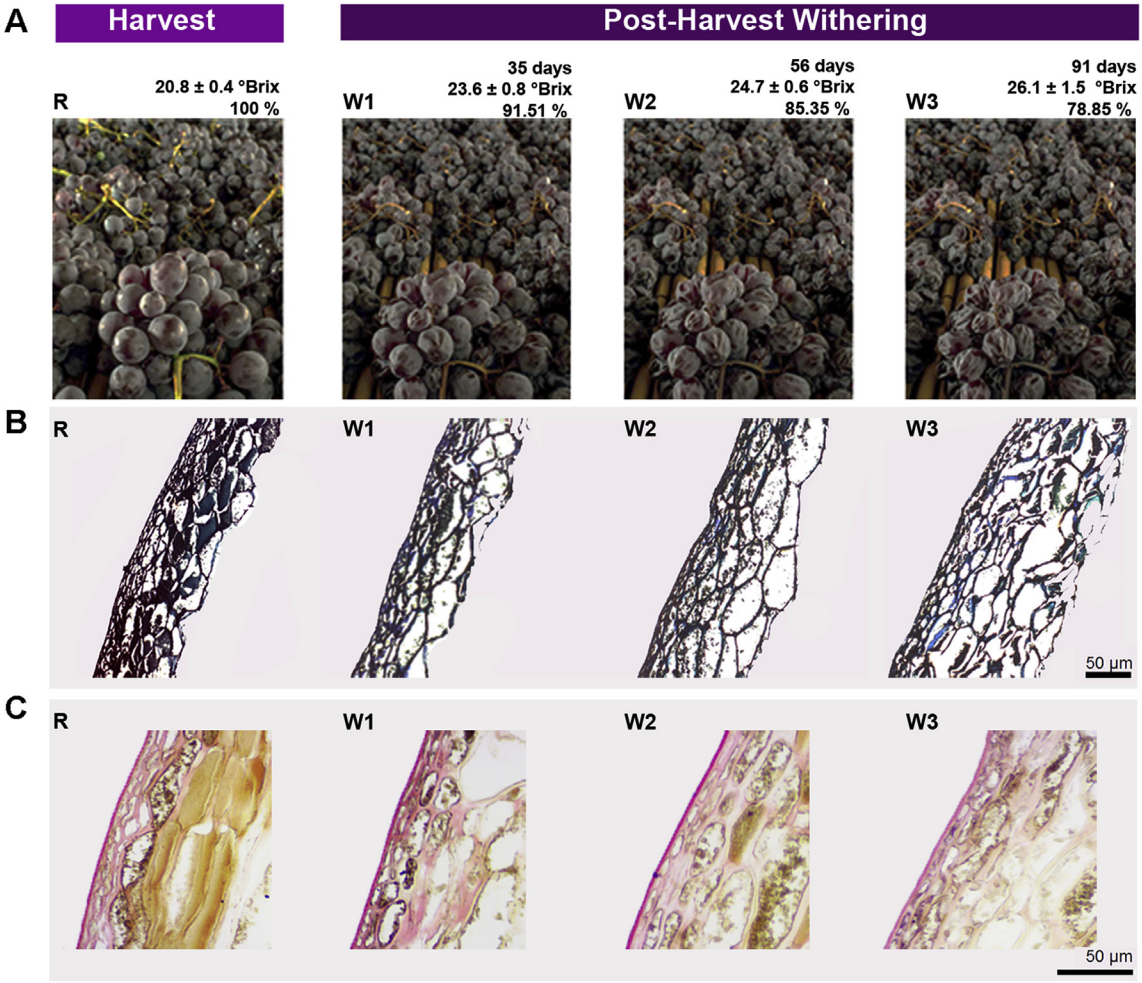

Fig. 2. Morphological alteration in the sampled berries. (A) Corvina berry clusters at full ripening (R) and postharvest withering stages (W1, W2 and W3). The number of days after harvest, the Brix degree (°Brix) and the percentage weight loss of the berries are reported. Brix degree values are expressed as mean ± s.d. (n = 7). **(B)** Toluidine blue staining on the transverse sections of the berry skin. Bars correspond to 50 µm. **(C)** Sudan IV staining on the transverse sections of the berry skin showing the epidermal cuticle layer and the hypodermal cutinized cells. This stain dyes lipids, triacylglycerols, and lipoproteins. Bars correspond to 50 µm. (For interpretation of the references to colour in this figure legend, the reader is referred to the Web version of this article.)

staining revealed a gradual cell disorganization from R to W3. It was previously observed that a progressive longitudinal expansion of the hypodermal cells characterized the ripening stages (Fasoli et al., 2016). Interestingly, a similar expansion of the hypodermal cells is also associated to the skin cell disorganization upon withering in the final stage from W2 to W3 (Fig. 2B).

The lipid-sensitive Sudan IV staining highlighted the cuticle and the hypodermal cutinized cells (Fig. 2C). Like with toluidine blue, the three withering stages show a progressive disaggregation of the different hypodermal cell layers that is mirrored by the gradual diffuse staining from R to W3. In addition, a slight difference was observed in the staining of the cuticle resulting less intense at stage W3 in comparison to the previous stages, although without no evident morphological difference (Fig. 2C).

3.2. FTIR spectra and main absorption bands in the berry skin during postharvest withering

To monitor polymer modifications in the berry skin, FTIR spectroscopy was performed on both the internal and external surfaces of the berry skins, following the same method as in our previous work on the berry ripening stages (Fasoli et al., 2016). Typical single-point absorbance spectra after baseline-correction and area-normalization are shown in Fig. 3A. Baseline-corrected and area normalized average spectra after selection for the full ripening stage and for the three withering stages, in the internal and in the external sides, are shown in Fig. 3B and C. Main absorption bands are related to the presence of functional chemical groups assigned to polyesters, water, amides, and cell wall polysaccharides (Table 1). The external surface of the berry skin was clearly distinguished by absorption bands previously assigned to cuticle polyesters and extracellular matrix structural proteins (Fasoli et al., 2016, Fig. 3B and C). Differently from the ripening stages, a band that we assigned to pectin galactans was identified at 1075 cm^{-1} in both the internal and external surfaces of the berry skin at the withering stages.

3.3. FTIR spectroscopy on the internal surface of the berry skin shows two processes characterized by a different time behaviour: water loss together with polymer concentration up to W2, and structural modifications involving xyloglucans and pectins occurring in the last phase of postharvest withering

PCA results for the area-normalized spectra on the internal surfaces of the berry skin at the full ripening stage (R) and over withering (W1, W2 and W3) are shown in Fig. 4. The four average spectra are distributed both on the PC1, which separates R from W1 and from W2/W3, and on the PC2, which interestingly mainly separates W3 from the other stages (Fig. 4A).

The PC1 loadings show a neat decrease from R to W2 in the water

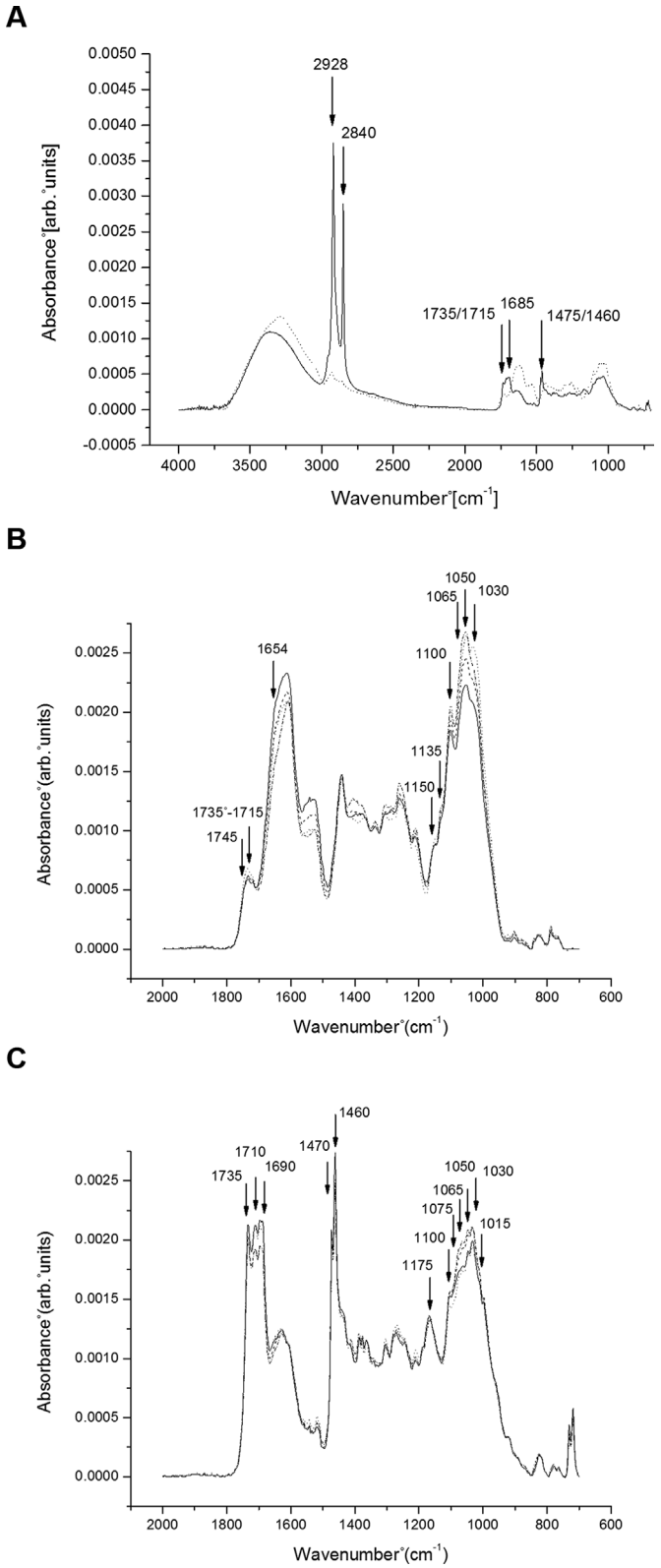

Fig. 3. FTIR spectra and main absorption bands. (A) Typical baseline-corrected and area-normalized spectra on the external (solid) and internal (dotted line) surfaces of the berry skin at the W1 post-harvest withering stage. The main cuticle-related absorption bands discussed in the text are reported. (**B**) Average baseline-corrected and area-normalized absorbance spectra in the 2000–700 cm^{-1} range after the selection procedure at R (solid line), W1 (dash line) W2 (dash-dot line) and W3 (dot line) acquired on the internal surface of the berry skin. The main absorption bands discussed in the text are reported. (**C**) Average baseline-corrected and area-normalized absorbance spectra in the 2000–700 cm^{-1} range after the selection procedure at R (solid line), W1 (dash line) W2 (dash-dot line) and W3 (dot line) acquired on the external surface of the berry skin. The main absorption bands discussed in the text are reported.

band at 1654 cm^{-1} (Fig. 4B), while in the PC2 loadings (where the band at 1644 cm^{-1} must be ascribed to amide I) there is no contribution from the 1654 cm^{-1} water band (Fig. 4C). This indicates that the process of water loss (hence polymer concentration) in the Corvina berry skin during withering ends up at W2. By comparing this finding with the steady loss of weight detected in the berry pericarps (Fig. 2A), it can be concluded that the process of water loss is faster in the skin than in the pulp. Interestingly, some biochemical processes, not simply related to polymer concentration but directly involving the relative polymer composition, are anyway present and detected in the PC2 (Fig. 4C).

To better highlight this polymer dynamics, the spectra acquired on the internal surface of the skin were normalized to the intensity of the adsorbed water band in the 1654–1649 cm^{-1} range indicated in Fig. 3B. The process of polymer concentration up to W2 is clearly confirmed by the PC1 showing that all the absorption bands increase (Fig. 5A and B). More precisely, the increase of xyloglucans (1130 cm^{-1} and 1065 cm^{-1} band) together with cellulose (1050 cm^{-1} and 1030 cm^{-1} band), prevails (Fig. 5B); there is also an increase in pectins (1100 cm^{-1} band) although with a lower loading value. Conversely, the PC2 highlights a biochemical-structural process occurring in the final stage between W2 and W3 (Fig. 5A and C). No dynamics related to cellulose is seen, whereas there is a decrease of xyloglucans (1130 cm^{-1} band and 1065 cm^{-1} band), and an increase of two pectin band (1100 cm^{-1} and 1015 cm^{-1}) and, to a lower extent, of their methylation (1740 cm^{-1} band). Interestingly, in the PC2 a decrease in the band at 1075 cm^{-1} (that we assigned to galactans) is also present, although with a low loading value (Fig. 5C).

3.4. FTIR spectroscopy on the external surface of the berry skin shows two processes characterized by a different time behaviour: polymer concentration up to W2, and structural modifications involving cuticle components, cellulose and pectins occurring in the last phase of postharvest withering

PCA results for the area-normalized spectra on the external surfaces of the berry skin at the full ripening (R) and at the three withering stages (W1, W2 and W3) are shown in Fig. 6A. In the PC1, a global identical time behaviour of cellulose (1050 cm^{-1} and 1030 cm^{-1} band), xyloglucans (1065 cm^{-1} band), galactans (1075 cm^{-1} band), and, to a lower extent, of the pectin 1100 cm^{-1} band prevails (Fig. 6A and B). These bands gradually increase from R to W2, suggesting a polymer concentration process similar to the internal surface one, then they all decrease to values comparable with R at W3 (Fig. 6B). This peculiar feature likely indicates a degradation of polymers at the W3 stage. Conversely, an opposite time behaviour, with lower loading values, is seen for the cuticle related bands which undergo a relative decrease up to W2 and then a relative increase to values similar to R at W3 (Fig. 6B). These observations suggest that the cuticle is not affected by the process of concentration related to water loss (up to W2) and that degradation (from W2 to W3) affects only polymers. This conclusion was supported by the PCA results obtained after normalization to the cuticle bands (Supplementary Fig. 1).

On the contrary, in the PC2, which is no more affected by the polymer concentration process prevailing in the PC1, a decrease between R and W3 in lipids and cuticle related bands (1735 cm^{-1}, 1685 cm^{-1}, 1475 cm^{-1} and 1460 cm^{-1}) is clearly detectable (Fig. 6A and C). In this respect, FTIR confirms what was evidenced by the Sudan colorimetric assay (Fig. 2C), providing a more detailed characterization of the structural modifications involving cuticle and epidermal

Table 1
Most meaningful absorption bands: assignments were based on the literature (Fasoli et al., 2016 and references therein).

Absorption bands (cm^{-1})	Main assignments
Bands related to the cuticle structure (waxes and structural proteins)	**Lipids and protein related vibrations**
~1735	C=O stretching in aliphatic polyesters (aldehydes)
~1715	C=O stretching in aliphatic polyesters (ketones)
~1685	Turn structures in amide I
Bands related to adsorbed water, amides and lipids	**Adsorbed water-related vibrations**
~1654	H−O−H bending in adsorbed water
~1645	Amide I
~1545	Amide II
~1475/1460	CH_2 asymmetric bending in lipids
Bands mainly related to cellulose	**Orientation sensitive cellulose-related vibrations**
~1175	C−O−C stretching modes of glycosidic bond in cellulose
~1050/1055	C−O stretching modes mainly of C_3− O_3H secondary alcohols in cellulose
~1030	C−OH stretching modes mainly of primary alcohols in cellulose
Bands mainly related to hemicellulose	**Hemicellulose related vibrations**
~1130/1135	$\beta_{1\text{-}3}$ glucans and C−O−C stretching modes of the glycosidic link in xyloglucans
~1065/1070	$\beta_{1\text{-}4}$ glucans and C−O and C−C stretching modes in xyloglucans

components. The PC2 is also sensitive to relative variations of cellulose, hemicellulose, and pectin. In particular, at W3 the xyloglucan 1135 cm^{-1} band undergoes only a slight increase. Conversely, two pectin bands (1150 cm^{-1} and 1100 cm^{-1}), decrease, while there is an increase in pectin methylation (1740 cm^{-1} band), which appears to be more pronounced than in the internal surface.

Interestingly, in the external surface, a decrease in the cellulose 1030 cm^{-1} and 1175 cm^{-1} bands is seen in the last stage, differently from the internal surface behaviour where no dynamics related to cellulose was detected. At the same time, the pectin galactan band at 1075 cm^{-1} also decreases.

A similar decrease in the galactan band between W2 and W3 was also found in the internal skin side, although to lower extent (Fig. 5C). Galactans, together with arabinans, are neutral chains of rhamnogalacturonan I (RGI) that represents, together with homogalacturonans, the most important types of pectin polysaccharides. Although the specific function of β-1,4-galactan in primary walls is poorly understood, it was suggested that β-1,4-galactans may represent a water retaining viscoelastic component with a likely role in modulating the mechanical properties of cell walls (Liwanag et al., 2012). This hypothetical function matches well with the observed decrease of galactans during postharvest withering in berry skin, a process which is strongly affected by water loss kinetics.

Moreover, galactans were demonstrated to strongly interact with cellulose microfibrils, supporting their role in transmitting stress to cellulose (Ulvskov et al., 2005; Zykwinska et al., 2007). Consistently with this hypothesis, we found a concomitant decrease of celluloses and galactans in the last stage of the external skin surface characterized by an extremely low water content.

To summarize, as a whole, present FTIR results suggest that in both the internal and external surfaces of the Corvina berry skin a passive polymer concentration process due to water loss occurs from R to W2, while a possibly active process characterized by structural polysaccharides modifications occurs in the final month of the withering process. This polymer rearrangement in the final stage involves xyloglucans in the internal surface, cuticle components and cellulose in the external surface, and pectins, with an increase of the methylated pectins and a decrease of galactans, in both the internal and external surfaces.

3.5. Immunohistochemistry evidences xyloglucans modifications occurring in the final stage of postharvest withering and different distribution of pectins with a low degree of methyl esterification in the external and in the internal skin surfaces

To corroborate and improve our interpretation of FTIR microspectroscopy results, immunohistochemical analyses were performed, like in our previous study on the berry skin during ripening (Fasoli et al., 2016). Sections of the berry skin at the same four stages (R, W1, W2, W3) were treated with CCRC-M1, CCRC-M58, JIM7 and LM19 monoclonal antibodies (Fig. 7) to examine hemicellulose and pectin dynamics. The signal of CCRC-M1 (Fig. 7A, B, C, D), which recognizes α-L-fucosylated xyloglucan, was mainly present in the internal layers and appeared more intense in W1 and W2, while it decreased in W3. A decrease of the labelling pattern in W3 was also found using CCRC-M58 antibody that recognizes non-fucosylated XG epitopes (Fig. 7E, F, G, H). These differences, although not quantitative, are in good agreement with FTIR results showing the decrease of xyloglucans, more pronounced in the internal side, in the final withering stage from W2 to W3 (Fig. 4).

As regards pectin localization, both JIM7 and LM19 antibodies bind to partially methyl esterified pectins, but JIM7 binds preferentially to pectin with a relatively high degree of methyl esterification, while LM19 binds preferentially to pectin with a relatively low degree of methyl esterification (Verhertbruggen et al., 2009). Similar to FTIR spectroscopy, immunohistochemistry showed that pectin dynamics involves both the internal and the external sides of the skin.

As regards JIM7 labelling, no significant differences were found between the internal and external skin surfaces (Fig. 7I, L, M, N) at any stage, suggesting a similar degree of methyl esterification. The JIM7 signal seemed slightly higher at the W3 stage compared with W1 and W2 in both surfaces. Conversely, the labelling with LM19 showed a higher signal in the external (epidermis) than in the internal (hypodermis) surface, with a decreasing signal towards the most internal layers (Fig. 7I, J, K, L). This suggests a different pattern of pectins with a low degree of methyl esterification in the internal and in the external skin surfaces at all stages. The labelling with LM19 showed complex dynamics during the withering process. The signal slightly increases in W1 compared with the full ripening stage (R), it decreases at W2 and then rises again in W3 becoming similar to the one observed at the R stage. This behaviour is more pronounced in the epidermis than in the hypodermis, where the signals in W2 and in W3 are instead quite comparable.

A similar dynamics of the pectin-related bands, differentiating between the internal and the external sides of the skin, was indeed detected also in the evolution of the PC1-PC2 scores in the FTIR analysis, where the PC2 mirrored an increase of methyl-esters in both sides of the berry skin, a decrease of the bands at 1100 cm^{-1} and 1150 cm^{-1} in the external surface (Fig. 6), and an increase of the bands at 1015 cm^{-1} and 1100 cm^{-1} in the internal surface (Figs. 4 and 5).

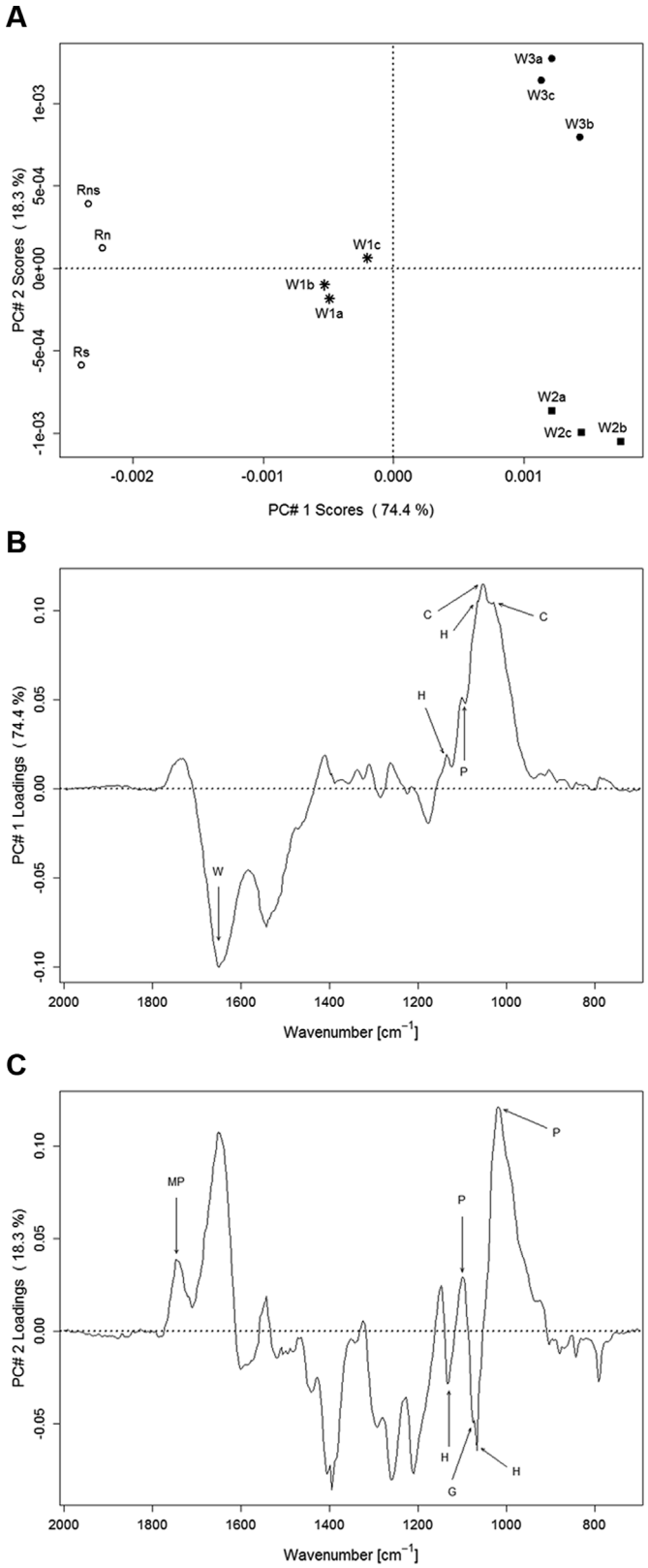

Fig. 4. PCA on the area-normalized average spectra in the 2000–700 cm^{-1} range for the three biological replicates at R, W1, W2, and W3 on the internal side of the berry skin. (A) PC1-PC2 score plot; **(B)** PC1 and **(C)** PC2 loading plot. In the loading plots, the arrows and letters indicate the relevant wavenumbers by the corresponding cell wall components, as reported in Table 1: H, hemicellulose; P, pectins; C, cellulose; MP pectin methylesters; G, galactans.

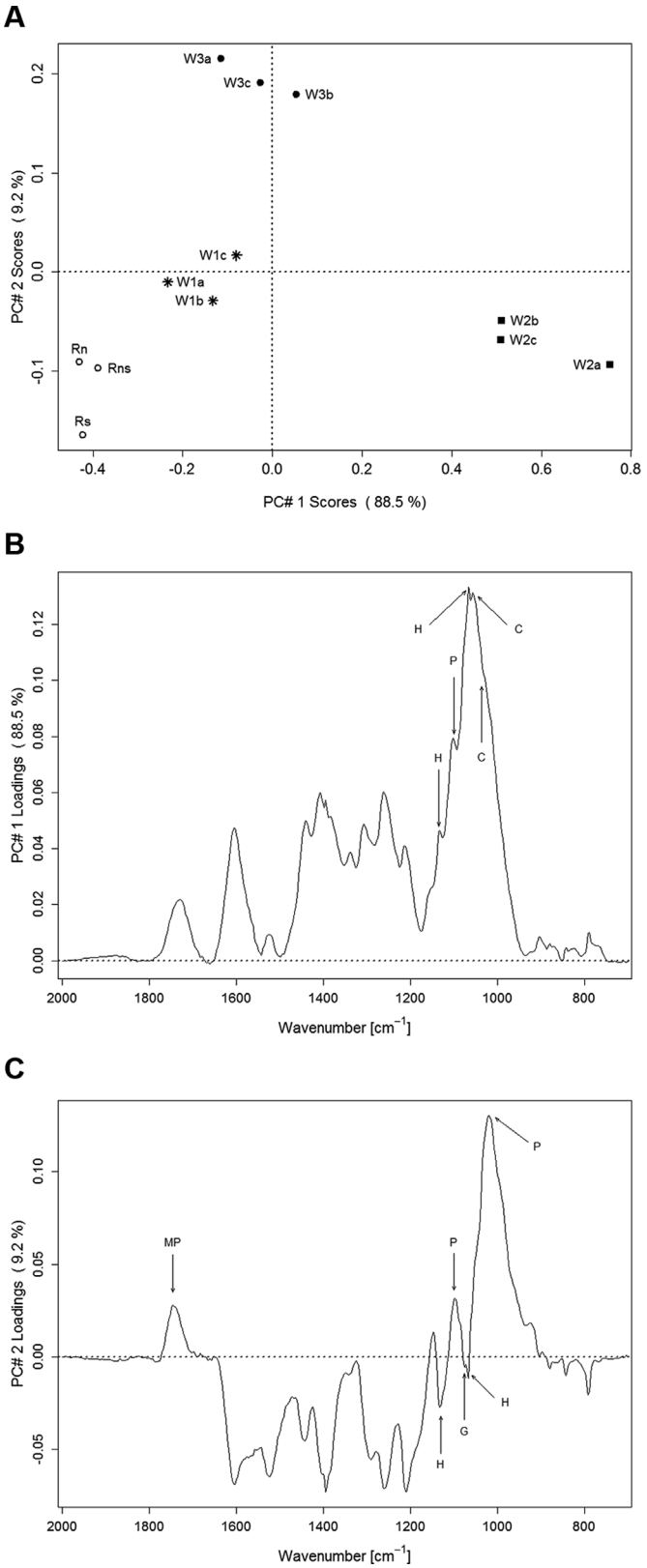

Fig. 5. PCA on the average spectra after normalization to the intensity of the adsorbed water band for the three biological replicates at R, W1, W2, and W3 on the internal side of the berry skin. (A) PC1-PC2 score plot; **(B)** PC1 and **(C)** PC2 loading plot. In the loading plots, the arrows and letters indicate the relevant wavenumbers by the corresponding cell wall components, as reported in Table 1: H, hemicellulose; P, pectins; C, cellulose; MP pectin methylesters; G, galactans.

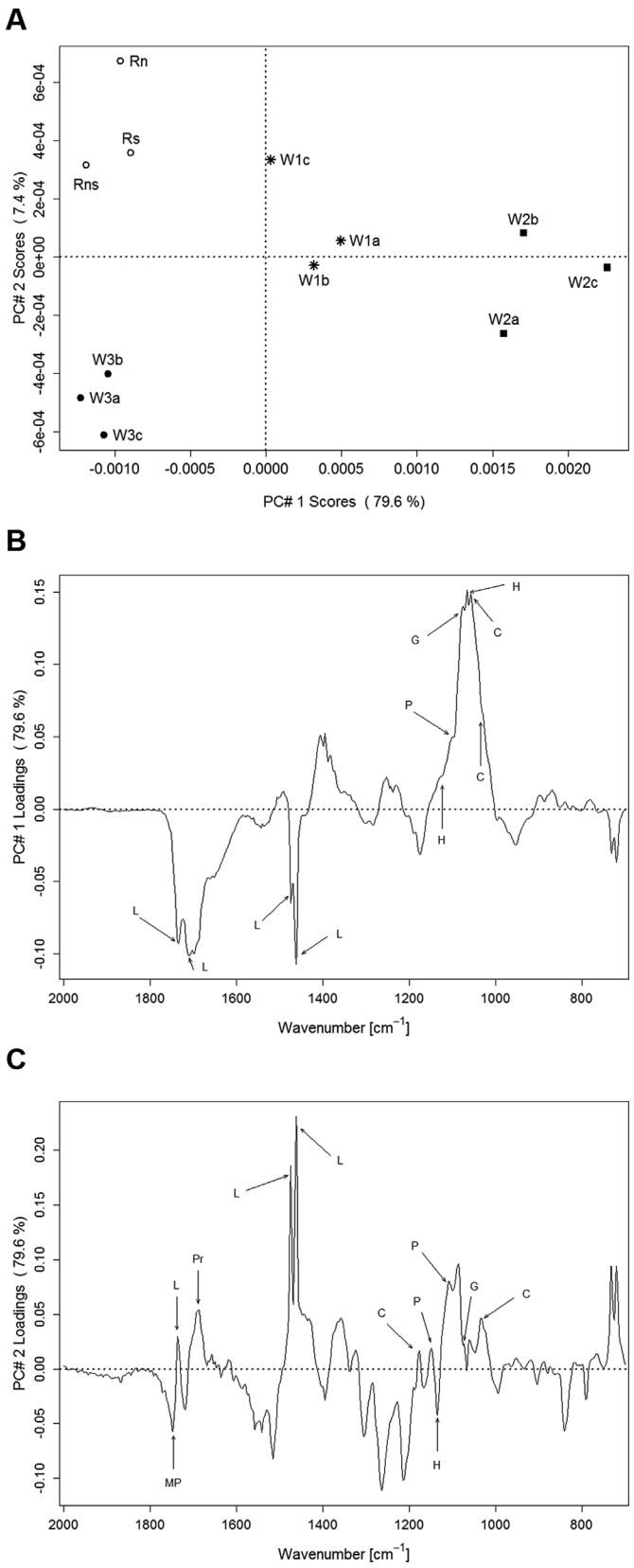

Fig. 6. PCA on the area-normalized average spectra for the three biological replicates at R, W1, W2, and W3 on the external side of the berry skin. (A) PC1-PC2 score plot; **(B)** PC1 and **(C)** PC2 loading plot. In the loading plots, the arrows and letters indicate the relevant wavenumbers by the corresponding cell wall components, as reported in Table 1: H, hemicellulose; P, pectins; C, cellulose; MP pectin methylesters; G, galactans; L, cuticle lipids; Pr, cuticle proteins.

3.6. Profiling the polymer metabolism-related genes in berry skin during postharvest withering evidences putative markers of the active polymers rearrangement

In order to investigate the molecular changes arising over withering in the berry skin and to identify putative markers involved in cell wall metabolism whose expression correlates with the polymer modifications seen by FTIR and immunohistochemistry, we explored the *V. vinifera* cv Corvina global expression atlas (Fasoli et al., 2012). This genome-wide survey distinguishes between flesh and skin of berry fruit tissues but not between external and internal surfaces of the skin. By applying SAM, GO manual selection and KMC analysis approaches, we obtained 81 cell wall-related genes, differentially expressed among the analysed phenological stages of the berry skin (Supplementary File S1). These were divided into five clusters of gene expression, among which Cluster 1, 2 and 3 exhibited active upregulation during the postharvest withering process, whereas Cluster 4 and 5 showed downward expression trends (Fig. 8). The highest number of differentially expressed genes (DEGs) belonged to Clusters 1 and 4. Interestingly, both clusters are characterized by a drastic change in the expression profiles of their genes within specific time ranges. In particular, genes belonging to Cluster 1 were promptly upregulated at the last stage of withering (W3), whereas the expression of genes belonging to Cluster 4 turned rapidly down after ripening (Fig. 8). This behaviour suggests that the major transcriptional changes of genes involved in cell wall metabolism occur during the transitions R−W1 and W2−W3.

Several genes involved in cell wall metabolism, i.e. xyloglucan rearrangement (15 xyloglucan endotransglucosylase/hydrolases (XTHs), one alfa 1–6, xylosyntransferase and two endo 1–3 1,4-β glucanases), pectin demethylation and degradation (four pectinesterases, three polygalacturonases and two pectate lyases) and general cell wall disassembly (several expansins and cell wall-related proteins) showed a downward expression trend during the withering process (Cluster 4 and 5; Fig. 8). Some of these genes were instead characterized by an increasing expression profile during the berry skin ripening, supporting their specific role in cell wall metabolism during berry maturation (Fasoli et al., 2016). Consistently, a general down regulation trend of the genes involved in cell wall metabolism was previously described in berry pericarp of six different genotypes dehydrated under identical environmental conditions (Zenoni et al., 2016). In the same study, as a general rule no cell wall metabolism-related genes were found to be upregulated during withering. Only in Corvina and Syraz cultivars a strong up-regulation of some pectin metabolism-related genes was found in the berry pericarp, suggesting that active cell wall rearrangement during postharvest withering is a genotype-specific trait (Zenoni et al., 2016).

As regards pectins, here we found that in the Corvina berry skin many genes were upregulated during withering: two pectinesterases, two pectate lyases and an exopolygalacturonase (Cluster 1), together with two pectinesterases and a pectinacetylesterase, which catalyzes the hydrolysis of acetate from acetylated pectin (Cluster 2; Fig. 8). The activity of these genes could be related to the decrease in the last stage of withering of bands related to galactans in both sides of the skin and to pectins in the external skin surface revealed by FTIR microspectroscopy. Interestingly, a specific pectinesterase (*VIT_15s0048g00500*) was found to be strongly upregulated during ripening in our previous survey (Fasoli et al., 2016), suggesting that its well-known role in regulating pectin demethylation is not withering-specific but is instead likely to be programmed from the beginning of ripening and to proceed during postharvest withering. In addition, a small contribution to pectin degradation in the external surface could be due to the activity of the polygalacturonase GH28 (Cluster 3) that showed a decrease in its expression after ripening followed by a slight increase at the end of the withering process (Fig. 8).

As regards xyloglucans, FTIR microspectroscopy revealed xyloglucan polymers degradation in the internal skin surface at the end of

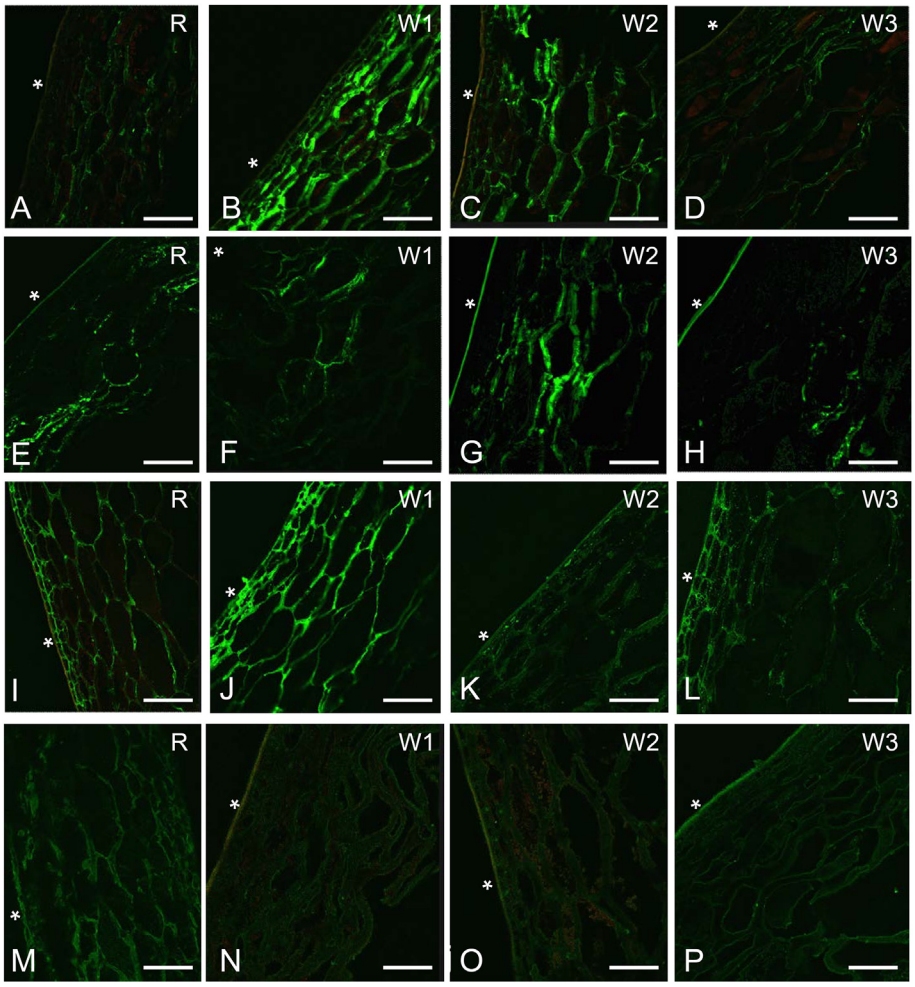

Fig. 7. Immunofluorescence labeling of pectins on paraffin sections of Corvina skins at R, W1, W2, and W3 time points. Immunofluorescence labeling was performed using the antibody CCRC-M1 (**A-D**) and CCRC-M58 (**E-H**) for xyloglucan (α-L-fucosylated and non-fucosylated, respectively), LM19 for de-esterified pectins (**J-L**) and JIM7 for highly esterified pectins (**M-P**). Treatment with CCRC-M1 led to a green signal, mainly present in the internal layers, that appeared more intense in W1 (**B**) and W2 (**C**), while decreased in W3 (**D**). CCRC-M58 led again to a signal in the internal layers in R, W1 and W2 (e–g), with a strong decreasing in W3 (**H**). Using LM19, the signal appears slightly higher in R, W1 and W3 (**I**, **J** and **L**, respectively) compared with the W2 stage (**K**). Treatment with JIM7 led to a signal on the cell wall that seems to be similar in the three withering stages (**N, O, P**) compared with the R stage (**M**). Scale bars correspond to 75 μm in A, E, I, K; 60 μm in B, J, N, O, P; 50 μm in C, D, F, G, H, L, M. In some photos, an autofluorescence is visible on the cutin layer. Asterisks pointed on the external surface. (For interpretation of the references to colour in this figure legend, the reader is referred to the Web version of this article.)

withering that was confirmed by immuno-histochemical analysis. Consistently with these results, we observed an up-regulation of two specific xyloglucan endotransglucosylase/hydrolase (Cluster 1 and 2) and of two endo-1,4-β-glucanase genes (Cluster 1 and 3) (Fig. 8). XTH genes encode for enzymes acting specifically on xyloglucans, in particular in the splitting and reconnection of xyloglucan cross-links of the cellulose-xyloglucan network (Han et al., 2015). As mentioned above, numerous XTH genes have been found to be downregulated during the withering process (Cluster 4; Fig. 8), and therefore the two genes of the family showing an active upregulation together with the two endo-1,4-β-glucanase genes involved in xyloglucan degradation could represent withering related molecular markers.

As regards cellulose dynamics, we found two cellulases (Cluster 1 and 2) and two cellulose synthases (CESAs, Cluster 1) involved in cellulose degradation and biosynthesis, respectively (Fig. 8). The decrease of cellulose-related bands observed between W2 and W3 in the external skin surface could be due to the action exerted by the two cellulases, whereas the induction of the two cellulose synthases could represents an active feedback response of berry skin cells even though the total cellulose content effectively decreases.

It is worth noting the strong activation of six β-1,3-glucanases belonging to Clusters 1 and to a lower extent to Cluster 3 at the last stage of postharvest withering (Fig. 8). The β-1,3-glucanases induction has been mainly referred to a response to pathogen infections, being their broad-spectrum antimicrobial activity associated to the hydrolysis of the fungal cell wall and to the callose turnover at plasmodesmata that impedes cell-to-cell virus movement in plants (Parre and Geitmann, 2005; Balasubramanian et al., 2012; Gupta et al., 2013). In addition, it was also reported that β-1,3-glucanases could be involved in the cryoprotection of the berry skin in red table grapes and a β-1,3-glucanase whose accumulation occurred at a chilling temperature was characterized in citrus (Sanchez-Ballesta et al., 2006; Romero et al., 2008). The mechanism underlying this hypothetical function of defence against chilling is not clear even though a similarity between antifreeze proteins and β-1,3-glucanases has been reported (Hon et al., 1995). To this respect, the cold winter temperature characterizing the last stage of the withering process, that ends up about three months after harvest, could explain the upregulation of the six β-1,3-glucanases in Corvina skin from W2 to W3.

Overall, although the gene expression analysis does not provide the layer-specific details observed using FTIR and immunohistochemical assays, our gene expression survey highlighted that no genes related to polymers biosynthesis are actively induced at the initial phases of the skin withering process. This observation corroborates FTIR results and strongly indicates that the R−W2 transition in mainly characterized by a passive concentration effect due to water loss.

On the other hand, transcriptomic profiling clearly confirms that postharvest withering involves also an active process driven by the modulation of cell wall metabolism related genes and allows to identify putative crucial molecular markers of cell wall metabolism representing an important quality trait of the dried berries.

4. Conclusions

To gain a more detailed understanding of cell wall biochemical changes and skin structure modifications occurring during postharvest withering, we studied this process in the berry skin of *Vitis vinifera* cv. Corvina, an important local variety of the Verona province in Italy. The

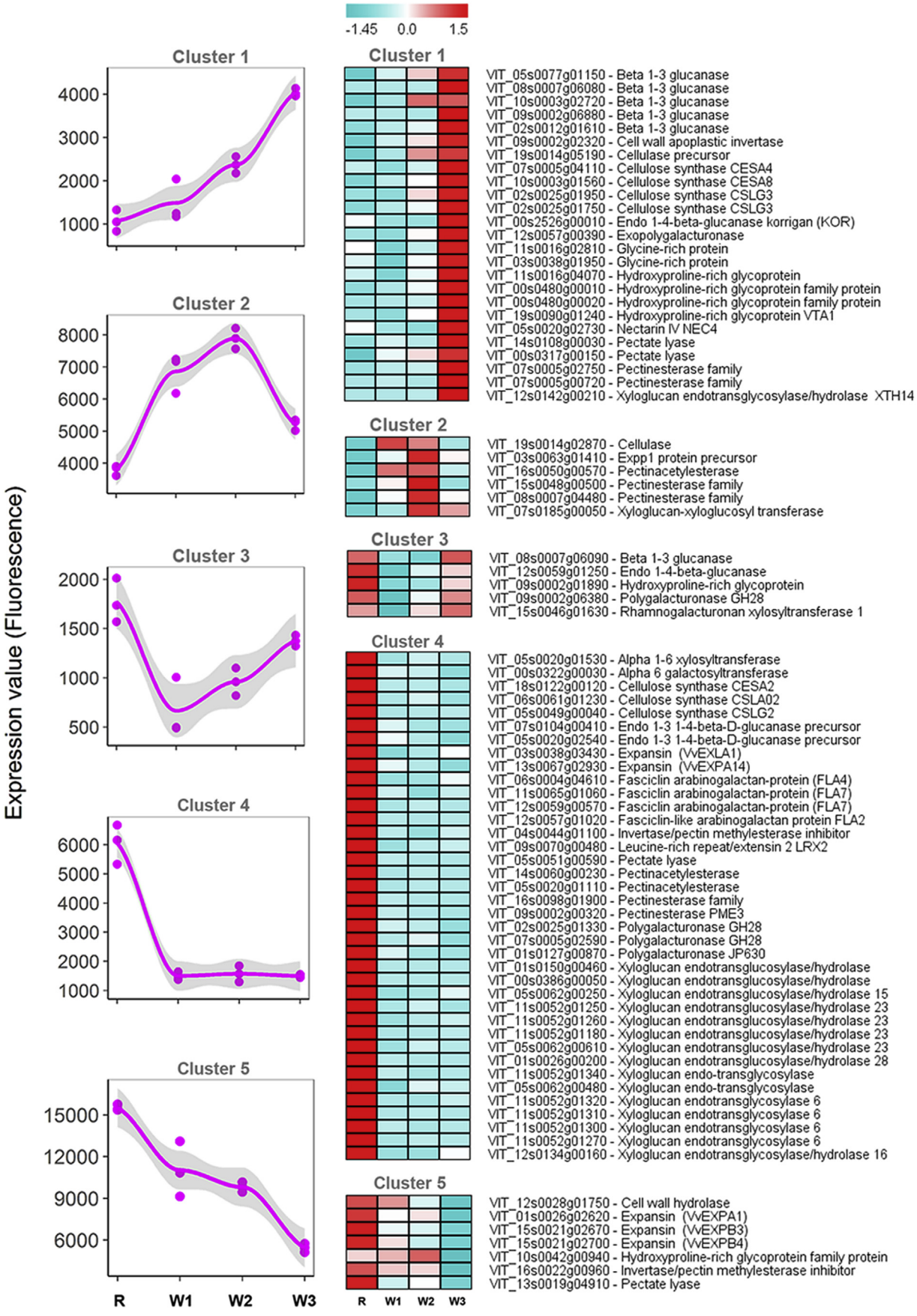

(caption on next page)

Fig. 8. Cell wall-related genes differentially expressed during the postharvest withering process in Corvina berry skin. Cell-wall-related differentially expressed genes were grouped by KMC analysis into 5 clusters of gene expression profiles. On the left, the averaged profiles of cluster-specific genes are plotted by days after harvest. On the right, in the heat map the expression was scaled by row and represented by colour scale intensity: azure and red boxes indicate low and high expression levels, respectively. Berry stages are indicated at the bottom of the line plots and heat maps representation and correspond respectively to samples at the four investigated stages (R, W1, W2 and W3) of the *Vitis vinifera* cv Corvina global expression atlas (Fasoli et al., 2012). (For interpretation of the references to colour in this figure legend, the reader is referred to the Web version of this article.)

dynamics of cell wall polysaccharides composition was investigated at three stages of the withering process using three different techniques: ATR-FTIR micro-spectroscopy on the internal and on the external surfaces of the berry skin, separately, immunohistochemistry on the skin sections, and global gene expression analysis on the whole berry skin. This multi-level approach allowed to reveal the distribution and evolution upon withering of the cell wall polymers and to relate the structural changes in polysaccharide composition to the gene expression. We demonstrated that this process is characterized by a gradual passive polysaccharide concentration due to water loss during the first two months, followed by an active process of structural modifications culminating in the third month of the withering process, driven by the modulation of cell wall metabolism related genes. The polymer rearrangement in the final stage mainly involves xyloglucans in the internal side, cuticle components and cellulose in the external side, an increase of methylated pectins and a decrease of pectin galactans in both the internal and external sides. Transcriptomic analysis corroborated FTIR and immunohistochemistry results and allowed to identify putative crucial molecular markers of cell wall metabolism representing an important quality trait of the dried berries.

Conflict of interest statement

The authors declare no conflict of interest.

Funding

This work was supported by the European Funded COST ACTION FA1106, the Joint Project 2011 between 'Pasqua vigneti e Cantine SpA' and the Biotechnology Department of the University of Verona, the Joint Project 2010 between 'Masi Agricola SpA' and the Biotechnology Department of the University of Verona.

Authors' contribution

Francesca Monti and Sara Zenoni designed and coordinated the research and oversaw manuscript writing. Marianna Fasoli performed the berry sampling and FTIR measurements, Alessandra Amato performed skin sections and optical microscopy and Raffaella Balestrini performed the immunofluorescence analyses. Rossana Dell'Anna and Silvia Dal Santo performed the statistical analyses on FTIR spectra and on transcriptomic data, respectively. Francesca Monti, Sara Zenoni and Rossana Dell'Anna gave the main contribution to the overall data interpretation. All the authors participated to writing the paper and to the discussion of the results and approved the final manuscript.

Acknowledgments

The authors want to thank Mara Novero for her assistance during confocal observations, Giorgio Pasqua for providing Corvina grapes, and Masi Agricola SpA for providing the dehydration room and pictures of grapes during withering.

List of abbreviations

ATR	attenuated total reflection
FTIR	Fourier transform infrared
PC	principal component
PCA	principal component analysis
PG	polygalacturonase
PME	pectin(methyl)esterase
SAM	significance analysis of microarray
XTH	xyloglucan endotransglucosylase/hydrolase

Appendix A. Supplementary data

Supplementary data to this article can be found online at https://doi.org/10.1016/j.plaphy.2018.11.020.

References

Alonso-Simón, A., García-Angulo, P., Mélida, H., Encina, A., Álvarez, J.M., Acebes, J.L., 2011. The use of FTIR spectroscopy to monitor modifications in plant cell wall architecture caused by cellulose biosynthesis inhibitors. Plant Signal. Behav. 6, 1104–1110.

Balasubramanian, V., Vashisht, D., Cletus, J., Sakthivel, N., 2012. Plant beta-1,3-glucanases: their biological functions and transgenic expression against phytopathogenic fungi. Biotechnol. Lett. 34, 1983–1990.

Barbanti, D., Mora, B., Ferrarini, R., Tornielli, G.B., Cipriani, M., 2008. Effect of various thermo-hygrometric conditions on the withering kinetics of grapes used for the production of "Amarone" and "Recioto" wines. J. Food Eng. 85, 350–358.

Bindon, K.A., Bacic, A., Kennedy, J.A., 2012. Tissue-specific and developmental modifications of grape cell walls influence the adsorption of proanthocyanidins. J. Agric. Food Chem. 60, 9249–9260.

Botondi, R., Lodola, L., Mencarelli, F., 2011. Postharvest ethylene treatment affects berry dehydration, polyphenol and anthocyanin content by increasing the activity of cell wall enzymes in Aleatico wine grape. Eur. Food Res. Technol. 232, 679–685.

Burattini, E., Cavagna, M., Dell'Anna, R., Malvezzi Campeggi, F., Monti, F., Rossi, F., Torriani, S., 2008. A FTIR microspectroscopy study of autolysis in cells of the wine yeast Saccharomyces cerevisiae. Vib. Spectrosc. 47, 139–147.

Cavagna, M., Dell'Anna, R., Monti, F., Rossi, F., Torriani, S., 2010. Use of ATR-FTIR microspectroscopy to monitor autolysis of Saccharomyces cerevisiae cells in a base wine. J. Agric. Food Chem. 58, 39–45.

Coombe, B.G., 1995. Growth Stages of the Grapevine: adoption of a system for identifying grapevine growth stages. Aust. J. Grape Wine Res. 1, 104–110.

Fasoli, M., Dell'Anna, R., Dal Santo, S., Balestrini, R., Sanson, A., Pezzotti, M., Monti, F., Zenoni, S., 2016. Pectins, hemicelluloses and celluloses show specific dynamics in the internal and external surfaces of grape berry skin during ripening. Plant Cell Physiol. 57, 1332–1349.

Fasoli, M., Dal Santo, S., Zenoni, S., Tornielli, G.B., Farina, L., Zamboni, A., Porceddu, A., Venturini, L., Bicego, M., Murino, V., Ferrarini, A., Delledonne, M., Pezzotti, M., 2012. The grapevine expression atlas reveals a deep transcriptome shift driving the entire plant into a maturation program. Plant Cell 24, 3489–3505.

Giacosa, S., Torchio, F., Segade, S.R., Caudana, A., Gerbi, V., Rolle, L., 2012. Varietal relationship between skin break force and off-vine withering process for winegrapes. Dry. Technol. 30, 726–732.

Griffiths, P., de Haseth, J.A., 1986. Fourier Transform Infrared Spectrometry. Wiley–Interscience Publishers, New York, USA.

Gupta, P., Ravi, I., Sharma, V., 2013. Induction of beta-1,3-glucanase and chitinase activity in the defense response of Eruca sativa plants against the fungal pathogen Alternaria brassicicola. J. Plant Interact. 8, 155–161.

Han, Y., Zhu, Q.G., Zhang, Z.K., Meng, K., Hou, Y.L., Ban, Q.Y., Suo, J.T., Rao, J.P., 2015. Analysis of xyloglucan endotransglycosylase/hydrolase (XTH) genes and diverse roles of isoenzymes during persimmon fruit development and postharvest softening. PloS One 10.

Hon, W.C., Griffith, M., Mlynarz, A., Kwok, Y.C., Yang, D.S.C., 1995. Antifreeze proteins in winter rye are similar to pathogenesis-related proteins. Plant Physiol. 109, 879–889.

Largo-Gosens, A., Hernandez-Altamirano, M., Garcia-Calvo, L., Alonso-Simon, A., Alvarez, J., Acebes, J.L., 2014. Fourier transform mid infrared spectroscopy applications for monitoring the structural plasticity of plant cell walls. Front. Plant Sci. 5, 303.

Liwanag, A.J.M., Ebert, B., Verhertbruggen, Y., Rennie, E.A., Rautengarten, C., Oikawa, A., Andersen, M.C.F., Clausen, M.H., Scheller, H.V., 2012. Pectin biosynthesis: GALS1 in Arabidopsis thaliana is a beta-1,4-galactan beta-1,4-galactosyltransferase. Plant Cell 24, 5024–5036.

Mencarelli, F., Bellincontro, A., Nicoletti, I., Cirilli, M., Muleo, R., Corradini, D., 2010. Chemical and biochemical change of healthy phenolic fractions in winegrape by means of postharvest dehydration. J. Agric. Food Chem. 58, 7557–7564.

Monti, F., Dell'Anna, R., Sanson, A., Fasoli, M., Pezzotti, M., Zenoni, S., 2013. A

multivariate statistical analysis approach to highlight molecular processes in plant cell walls through ATR FT-IR microspectroscopy: the role of the α-expansin PhEXPA1 in Petunia hybrida. Vib. Spectrosc. 65, 36–43.
Moore, J.P., Fangel, J.U., Willats, W.G., Vivier, M.A., 2014a. Pectic-beta(1,4)-galactan, extensin and arabinogalactan-protein epitopes differentiate ripening stages in wine and table grape cell walls. Ann. Bot. 114, 1279–1294.
Moore, J.P., Nguema-Ona, E., Fangel, J.U., Willats, W.G., Hugo, A., Vivier, M.A., 2014b. Profiling the main cell wall polysaccharides of grapevine leaves using high-throughput and fractionation methods. Carbohydr. Polym. 99, 190–198.
Oliveira, H., Barros, A.S., Delgadillo, I., Coimbra, M.A., Santos, C., 2009. Effects of fungus inoculation and salt stress on physiology and biochemistry of in vitro grapevines: emphasis on sugar composition changes by FT-IR analyses. Environ. Exp. Bot. 65, 1–10.
Ortega-Regules, A., Romero-Cascales, I., Ros-García, J.M., López-Roca, J.M., Gómez-Plaza, E., 2006. A first approach towards the relationship between grape skin cell-wall composition and anthocyanin extractability. Anal. Chim. Acta 563, 26–32.
Paronetto, L., Dellaglio, F., 2011. Amarone: a modern wine coming from an ancient production technology. Adv. Food Nutr. Res. 63, 285–306.
Parre, E., Geitmann, A., 2005. More than a leak sealant. The mechanical properties of callose in pollen tubes. Plant Physiol. 137, 274–286.
Rizzini, F.M., Bonghi, C., Tonutti, P., 2009. Postharvest water loss induces marked changes in transcript profiling in skins of wine grape berries. Postharvest Biol. Technol. 52, 247–253.
Rolle, L., Gerbi, V., 2013. Changes in physical and mechanical properties of dehydrating berries. In: F Mencarelli, E.T. (Ed.), Sweet, Reinforced and Fortified Wines. Wiley-Blackwell, Hoboken, NJ, USA.
Rolle, L., Torchio, F., Giacosa, S., Gerbi, V., 2009. Modifications of mechanical characteristics and phenolic composition in berry skins and seeds of Mondeuse wine-grapes throughout the on-vine drying process. J. Sci. Food Agric. 89, 1973–1980.
Rolle, L., Segade, S.R., Torchio, F., Giacosa, S., Cagnasso, E., Marengo, F., Gerbi, V., 2011. Influence of grape density and harvest date on changes in phenolic composition, phenol extractability indices, and instrumental texture properties during ripening. J. Agric. Food Chem. 59, 8796–8805.
Romero, I., Fernandez-Caballero, C., Goni, O., Escribano, M.I., Merodio, C., Sanchez-Ballesta, M.T., 2008. Functionality of a class I beta-1,3-glucanase from skin of table grapes berries. Plant Sci. 174, 641–648.
Sanchez-Ballesta, M.T., Gosalbes, M.J., Rodrigo, M.J., Granell, A., Zacarias, L., Lafuente, M.T., 2006. Characterization of a beta-1,3-glucanase from citrus fruit as related to chilling-induced injury and ethylene production. Postharvest Biol. Technol. 40, 133–140.
Team, R.C., 2015. R: a Language and Environment for Statistical Computing. R Foundation for Statistical Computing, Vienna, Austria URL: http:/www.R-project.org/.
Ulvskov, P., Wium, H., Bruce, D., Jorgensen, B., Qvist, K.B., Skjot, M., Hepworth, D., Borkhardt, B., Sorensen, S.O., 2005. Biophysical consequences of remodeling the neutral side chains of rhamnogalacturonan I in tubers of transgenic potatoes. Planta 220, 609–620.
Verhertbruggen, Y., Marcus, S.E., Haeger, A., Ordaz-Ortiz, J.J., Knox, J.P., 2009. An extended set of monoclonal antibodies to pectic homogalacturonan. Carbohydr. Res. 344, 1858–1862.
Versari, A., Parpinello, G.P., Tornielli, G.B., Ferrarini, R., Giulivo, C., 2001. Stilbene compounds and stilbene synthase expression during ripening, wilting, and UV treatment in grape cv. Corvina. Journal of agricultural and food chemistry 49, 5531–5536.
Vicens, A., Fournand, D., Williams, P., Sidhoum, L., Moutounet, M., Doco, T., 2009. Changes in polysaccharide and protein composition of cell walls in grape berry skin (Cv. Shiraz) during ripening and over-ripening. J. Agric. Food Chem. 57, 2955–2960.
Vincenzi, S., Tolin, S., Cocolin, L., Rantsiou, K., Curioni, A., Rolle, L., 2012. Proteins and enzymatic activities in Erbaluce grape berries with different response to the withering process. Anal. Chim. Acta 732, 130–136.
Wickham, H., 2009. ggplot2: Elegant Graphics for Data Analysis. Springer-Verlag, New York.
Zamboni, A., Minoia, L., Ferrarini, A., Tornielli, G.B., Zago, E., Delledonne, M., Pezzotti, M., 2008. Molecular analysis of post-harvest withering in grape by AFLP transcriptional profiling. J. Exp. Bot. 59, 4145–4159.
Zenoni, S., Fasoli, M., Guzzo, F., Dal Santo, S., Amato, A., Anesi, A., Commisso, M., Herderich, M., Ceoldo, S., Avesani, L., Pezzotti, M., Tornielli, G.B., 2016. Disclosing the molecular basis of the postharvest life of berry in different grapevine genotypes. Plant Physiol. 172, 1821–1843.
Zoccatelli, G., Zenoni, S., Savoi, S., Dal Santo, S., Tononi, P., Zandonà, V., Dal Cin, A., Guantieri, V., Pezzotti, M., Tornielli, G.B., 2013. Skin pectin metabolism during the postharvest dehydration of berries from three distinct grapevine cultivars. Aust. J. Grape Wine Res. 19, 171–179.
Zykwinska, A., Thibault, J.F., Ralet, M.C., 2007. Organization of pectic arabinan and galactan side chains in association with cellulose microfibrils in primary cell walls and related models envisaged. J. Exp. Bot. 58, 1795–1802.